The Journal of Experimental Biology 207, 4255-4268
Published by The Company of Biologists 2004
doi:10.1242/jeb.01283

The relationship between wingbeat kinematics and vortex wake of a thrush nightingale

M. Rosén[1,*,†], G. R. Spedding[2] and A. Hedenström[1,‡]

[1]*Department of Animal Ecology, Lund University, Ecology Building, SE-223 62 Lund, Sweden* and [2]*Department of Aerospace and Mechanical Engineering, University of Southern California, Los Angeles, CA 90089-1191, USA*

*Author for correspondence (e-mail: m.rosen@usc.edu)

†Present address: Department of Aerospace and Mechanical Engineering, University of Southern California, Los Angeles, CA 90089-1191, USA

‡Present address: Department of Theoretical Ecology, Lund University, Ecology Building, SE-223 62 Lund, Sweden

Accepted 14 September 2004

Summary

The wingbeat kinematics of a thrush nightingale *Luscinia luscinia* were measured for steady flight in a wind tunnel over a range of flight speeds (5–10 m s^{-1}), and the results are interpreted and discussed in the context of a detailed, previously published, wake analysis of the same bird. Neither the wingbeat frequency nor wingbeat amplitude change significantly over the investigated speed range and consequently dimensionless measures that compare timescales of flapping *vs.* timescales due to the mean flow vary in direct proportion to the mean flow itself, with no constant or slowly varying intervals. The only significant kinematic variations come from changes in the upstroke timing (downstroke fraction) and the upstroke wing folding (span ratio), consistent with the gradual variations, primarily in the upstroke wake, previously reported.

The relationship between measured wake geometry and wingbeat kinematics can be qualitatively explained by presumed self-induced convection and deformation of the wake between its initial formation and later measurement, and varies in a predictable way with flight speed. Although coarse details of the wake geometry accord well with the kinematic measurements, there is no simple explanation based on these observed kinematics alone that accounts for the measured asymmetries of circulation magnitude in starting and stopping vortex structures. More complex interactions between the wake and wings and/or body are implied.

Key words: wingbeat kinematics, vortex wake, thrush nightingale, *Luscinia luscinia*, DPVI, aerodynamics, bird flight, bird, wind tunnel.

Introduction

An extensive set of experiments on the flight aerodynamics of a thrush nightingale *Luscinia luscinia* L. were described by Spedding, Rosén and Hedenström (2003a), giving detailed quantitative measurements of the wake. The wake structure was complex, but the gradual changes in circulation of cross-stream or spanwise wake elements and inferred changes in three-dimensional (3D) wake topology supported an empirical model that was self-consistent and provided sufficient averaged vertical forces to balance weight in steady flight. Since no previous quantitative wake measurements have been reported at more than one flight speed for any particular bird (or bat) species, the observations of change in structure with flight speed as an independent, controllable parameter were new, interpolating some rather large gaps in the literature.

A notable characteristic of aerodynamic studies using wake analysis is that the results do not depend on, or reveal anything directly about, the wing kinematics that create the disturbance. While observations of wake structure were new and extensive, they were related to the kinematics only by rather loose inference. The kinematic basis for flight in birds and bats has a long history of careful measurement (see, for example, Brown 1953; Norberg, 1976) for classic treatments of birds and bats, respectively). In turn, inferring aerodynamic quantities from kinematics alone is also difficult. In the absence of any better alternative, all such studies have been obliged to make strong assumptions about the quasi-steady (and 2D) aerodynamic properties of the wing sections as they accelerate and deform during the wingbeat. A more recent study by Hedrick et al. (2002) carried these calculations through to the point of estimating circulations of wing sections, but this process invoked exactly the same set of quasi-steady assumptions about how the wing motion and air flow are linked. Undoubtedly, much remains to be done to make this connection clearer. This paper is a small step in this direction, where a simple kinematic analysis is related to the measured wake flow. The flow on the wing itself is inaccessible to the flow experiments, but correlates of kinematic variation with wing speed and wake structure will be sought.

The wingbeat kinematics were analysed for the same bird under similar conditions as for the wake study. As in the wake measurements, it is critical that the flight training be sufficient to ensure consistent, repeatable, steady flight over the whole range of studied flight speeds. The kinematic analysis allows this requirement to be checked, and more importantly, for the changing wake structure to be correlated with observed changes in kinematics. This study becomes more compelling in light of the rather complex wake structures revealed in the wake analysis of Spedding, Rosén and Hedenström (2003a).

Materials and methods

Bird and flight training

The thrush nightingale *Luscinia luscinia* L. is a typical migrating songbird with a rather low aspect ratio $\mathcal{AR}$, i.e. length to width ratio of the wing ($\mathcal{AR}$=5.4), body mass ≈30 g and an annual migration between its breeding range in Europe and wintering range in south-east Africa (Moreau, 1972).

Initially four juvenile thrush nightingales were caught at Ottenby Bird Observatory, Sweden, on their autumn migration in August 2001. After 2 weeks of flight training, it became clear that one bird was far more capable of prolonged and stable flights. This bird was further trained to perch on a stick mounted on the wind tunnel sidewall when not flying. During flight tests, the stick was manually tilted downwards to initiate flight. About 1 m upstream from the perch location a luminous marker was placed in the airflow to serve as a reference point for where the perch would reappear at the end of a flight episode. The marker helped to direct the flight position of the bird to the centre of the test section and repeated trials over 3 months converged towards stable and repeatable flights.

When running flow visualisation experiments the bird would fly in reduced light conditions as required for the digital particle image velocimetry (DPIV) measurements, but the high speed camera recordings required about 2 kW of continuous light. The thrush nightingale is a typical nocturnal migrant and preferred the dark settings, as reflected in the broader range of flight speeds recorded (4–11 m s^{-1} in low-light conditions compared with 5–10 m s^{-1} by the high-speed cameras). Previous experiments using thrush nightingales in the same wind tunnel have produced the same range of observed flight speeds as for this set-up, 5–10 m s^{-1} (e.g. Pennycuick et al., 1996). Here, in the digital video recordings, a typical flight episode would last for 10–30 s (limited by the bird's accurate flight position in the test section), followed by a few minutes of rest on the perch. The cycle could be repeated for about 90 min before the bird was put back in the aviary for a longer rest. Typically one morning and one afternoon flight session were performed each day. In total the training was scheduled daily for 3 months prior to the start of experiments. The experiments using flow visualisation and high-speed cameras lasted for another 50 days (end 11 January, 2002). The bird was released into the wild the following spring, seemingly unaffected by the experience. For bird morphological characteristics, see Table 1.

Sampling and analysis of wingbeat kinematics

The number of steady flight episodes analysed at each flight speed U were 5, 5, 5, 4, 5 and 4 at 1 m s^{-1} intervals from 5 to 10 m s^{-1}.

A RedLake digital video camera system (MotionScope PCI500, USA, operating at frame rate 125 s^{-1}, shutter speed 1/1850 s) was mounted 4 m downstream from the bird's flight position. The location of the camera far back in the first diffuser causes a negligible effect on the airflow around the bird (see Pennycuick et al., 1997). From the camera AVI-output, strings of JPEGs were extracted and used for the analysis.

Time sequences of y, z coordinates (Fig. 1A) of the wingtip and shoulder joint for both wings (mean presented) were digitised using a custom program written in PV-WAVE (Visual Numerics, USA) command language, the same language used for accessing and calculating quantities in the wakes database. The body width was used as a reference length scale to calculate physical distances.

The projected wingspan $b'(t)$ (m), was measured from tip to tip, throughout the wingbeat cycle. b'_{d} is the projected span at mid downstroke ±10° from horizontal (Fig. 1A). The horizontal position is defined as a line connecting the left and right shoulder joints. b'_{u} is the equivalent measure for the upstroke (Fig. 1A). In the upstroke the wing is moving rapidly, almost vertically, so registrations of the wingtip in the horizontal position are scarce and the data were interpolated graphically from a diagram of $b'(y,z)$ constructed from $b'(t)$ sequences. The span ratio, R, is calculated from

$$R = b'_{\mathrm{u}} / b'_{\mathrm{d}} . \quad (1)$$

The wingtip position in the vertical z_{tip} was calculated as the vertical distance between the wingtip and the horizontal line, hence z_{tip}=0 is a wing held in the horizontal position (Fig. 1A). The beginning and end of a wing stroke were defined as the points where z_{tip} reaches maximum values above ($z_{\mathrm{tip,max}}$) and below ($z_{\mathrm{tip,min}}$) the horizontal, respectively (Fig. 1A). The downstroke ratio τ is the ratio of the downstroke duration to the total stroke period where start and stop points of the downstroke and upstroke were determined by the maximum and minimum values of z_{tip}.

The wingbeat frequency f and wingbeat amplitude, A_1, were derived from fitting a single frequency sine function to the wingtip trace, so the vertical direction of the wingtip is described by

$$z_{\mathrm{tip}}(t) = A_0 + A_1 \sin(\omega t + \varphi) , \quad (2)$$

Table 1. *Morphological characteristics of the thrush nightingale*

	Symbol	Mean value	Units
Body mass	m	0.030	kg
Semi span	b	0.131	m
Wing area	S	0.0126	m^2
Aspect ratio	$\mathcal{AR}$	5.4	
Mean chord	c	0.048	m
Wing loading	Q	23	N m^{-2}

where A_0 is the offset of the wingbeat, A_1 is the amplitude (which varies from $+A_1$ to $-A_1$), ω is the radian frequency $2\pi f$ and φ is the arbitrary phase offset to account for initial phase value of the sequence. This measure of amplitude in the tunnel-fixed reference frame (rather than body-fixed coordinates) does not account for variations in the body tilt angle and hence underestimates the wingtip excursion relative to the body at low speeds when the body tilt angle increases. However, it is the tunnel reference frame that can be more simply related to the wake geometry in Spedding, Rosén and Hedenström (2003a).

$1/f$, the stroke period, is denoted T. The horizontal stroke wavelength λ (see Fig. 1B) of a wingbeat cycle was calculated from wingbeat frequency and speed U as

$$\lambda = (1/f)U = TU \, . \tag{3}$$

The reduced frequency k is proportional to the ratio of two time scales, the average time required for the mean flow to pass over the mean chord, $t_c=c/U$, and the time taken for one wingbeat, $T=1/f$. It is conventionally expressed in terms of the mean half chord, $c/2$, and radian frequency, $\omega=2\pi f$, as

$$k = \omega c / 2U \, . \tag{4}$$

The magnitude of k is frequently used as an indicator of the relative importance of unsteady terms in the aerodynamics, and in classical, small amplitude theories, it is exactly this (e.g. Theodorsen, 1934). Some caution is due in a simple-minded application of this number to complex geometries and kinematics of animal flight, but very generally when k is on the order of 0.1 then unsteady effects can usually be ignored, while k of order 1 signals a probable strong influence of unsteady phenomena (see also remarks by Spedding, 1993).

A similar measure, K, can be constructed from the ratio of mean tip speed in the vertical (w_{tip}) to forward flight speed:

$$K = w_{tip} / U \, . \tag{5}$$

Since the arc length s travelled by the wingtip is $s=\phi b$, and this is accomplished twice per wingbeat cycle, then

$$w_{tip} = 2\phi bf \, ,$$

and

$$K = 2\phi bf / U \, . \tag{6}$$

Note that K incorporates a measure of the wingbeat amplitude through the inclusion of the stroke angle, ϕ. The inverse of K is commonly encountered as the advance ratio, J, and when written

$$J = K^{-1} = UT / 2\phi b \, , \tag{7}$$

it can be seen that when $J=K=1$, the forward distance travelled per wingbeat, UT, is equal to the distance traced by the tip with respect to the body.

The measured inclination angles of the wingtip trace are $\psi_{kin,d}$ and $\psi_{kin,u}$ (deg.) for the down- and upstrokes (Fig. 1B), respectively. Values for ψ_{kin} are calculated from $2A_1$ and λ as

$$\psi_{kin} = \arctan(2A_1/\lambda) \, , \tag{8}$$

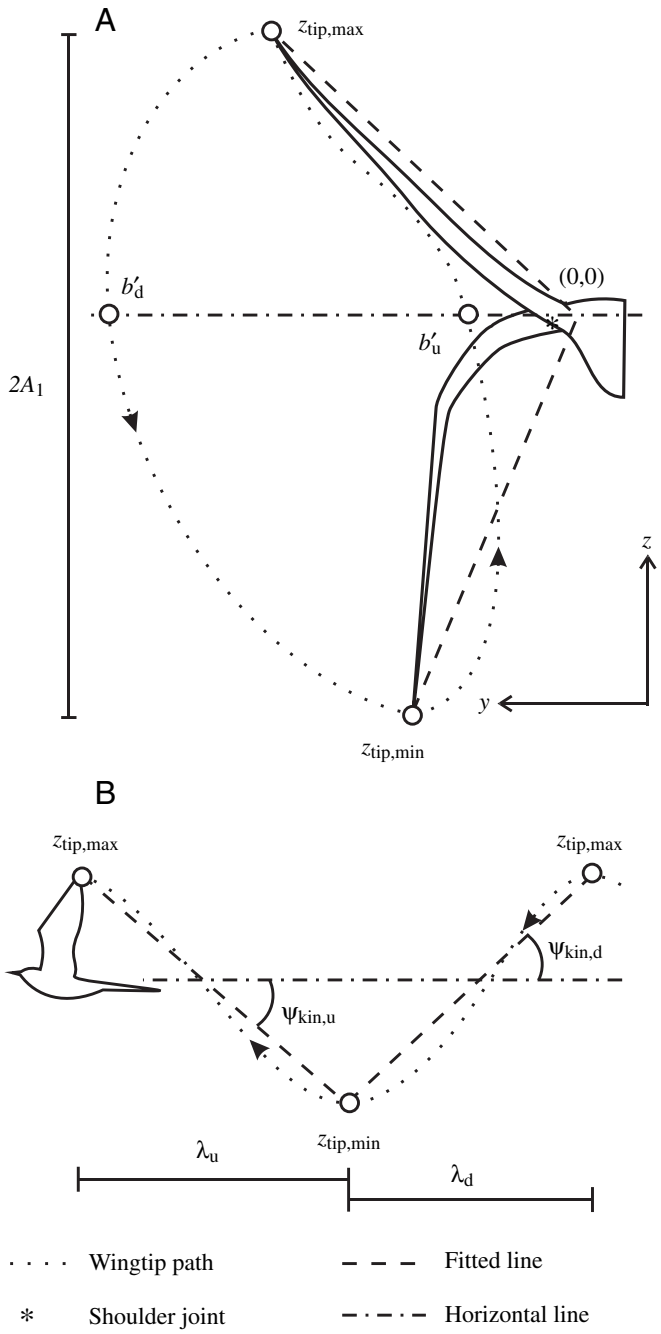

Fig. 1. Schematic drawing to show how kinematics were measured from the wingtip trace. (A) Bird in rear view. z_{tip} is the vertical position of the wingtip at any instance of the wingbeat. When the wingtip is at a maximum vertical distance from the horizontal, $z_{tip,max}$ and $z_{tip,min}$ are defined. The amplitude A_1 (m), was derived from fitting a single frequency sine function to the wingtip trace, hence $2A_1$ represents the peak-to-peak swing of the wingtip over a full wingbeat. The projected wingspan, b′, is measured from tip to tip. When the wing is in the horizontal position at downstroke b'_d is measured. Similarly, b'_u is measured in horizontal position for the upstroke. The span ratio $R=b'_u/b'_d$. (B) Side view of the flight path through still air. The inclination angle ψ of the wingtip path to the horizontal line was calculated from a line fitted between $z_{tip,max}$ and $z_{tip,min}$ for the upstroke $\psi_{kin,u}$ and downstroke $\psi_{kin,d}$ separately. Stroke wavelength λ is the distance the wingtip travelled during downstroke, λ_d, and upstroke, λ_u.

using λ_d and λ_u for wavelengths of downstroke and upstroke, respectively (Fig. 1B).

Measuring the wake topology

The method used for estimating the velocity field behind a bird in the wind tunnel is described by Spedding et al. (2003b) and this particular analysis of the thrush nightingale is accounted for in detail by Spedding, Rosén and Hedenström (2003a).

Inclination angles of the wake

The inclination angle of the wake was estimated using two different methods:

Method 1: wake trace

The flapping wings generate sections of wake on the down and upstroke that can be reasonably well approximated as plane sections (Spedding, Rosén and Hedenström, 2003a) (ψ_{trace}, Fig. 2). The inclination angle of these sections was estimated by drawing a line parallel to the section plane. At low speeds this section is defined by a line from the centre of the start vortex Γ+ to the centre of the dominating (stop) vortex Γ– at the end of downstroke. ψ_{trace} is the angle between this line and the horizontal. At higher speeds, where a full stroke wavelength could not be captured in a single image, a line was fit to the wake trace originating from a mid up- or downstroke.

Method 2: induced flow

Alternatively, the mean inclination angle could be taken from a line normal to the direction of induced downwash at the centre of the vortex structure (ψ_{ind}, Fig. 2). So derived, ψ_{ind} may be supposed to be a reasonable measure of the average direction of the mean resultant force from that part of the wingbeat. When the induced flow is normal to the wake plane, then $\psi_{ind}=\psi_{trace}$.

ψ_{ind} and ψ_{trace} were measured from upstroke and downstroke segments separately using wake data sampled behind the mid-wing position and central-body position only (Spedding, Rosén and Hedenström, 2003a). The analysis included only segments of the wake that were typical for steady flight.

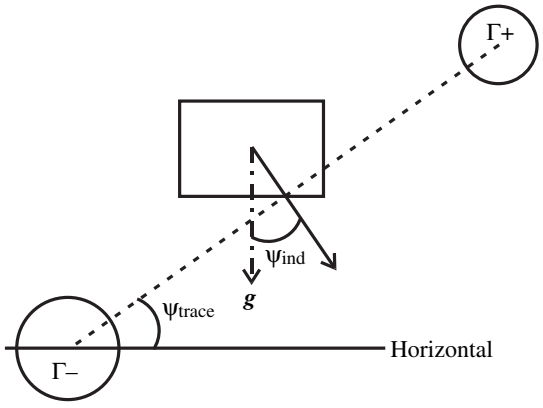

Fig. 2. Schematic drawing of the vertical centreplane cross section of a wake generated by a downstroke at low speed. The positive start vortex and the negative stop vortex are indicated as circles. The inclination angle of the wake plane, ψ_{trace}, with respect to the horizontal was obtained by fitting a straight line between the start (Γ+) and stop vortex (Γ–) at low speeds and a line parallel to the wake trace at intermediate and high speeds. The direction of the induced downwash was estimated from an average in a rectangular box in the centre of the wake just above the wake trace. The inclination angle of the induced downwash (ψ_{ind}) was then calculated relative to the vertical.

Results

Characteristic results

The flight of the thrush nightingale (in both kinematic and wake experiments) was characterised by indicators of stable and relaxed flight. The bird had a closed bill and the head was moving up and down in synchrony with the beating motion of the wings, as is typical of natural flight in birds observed in the wild, i.e. it was not flying with the head fixed in space as when manoeuvring. The feet were fully tucked up and the tail furled at higher speeds as typical for cruising flight. Although quantifiable differences in degree exists, the most striking qualitative feature is the similarity of the kinematics across the full range of flight speeds (Fig. 3). The strongly pronated leading edge is in shade during the downstroke, whose progress can be followed in the right-hand columns of Fig. 3A–C, where U=5, 7 and 10 m s^{-1}, respectively. During this time the wings are almost fully extended. The wings are then sharply flexed during the ensuing upstroke. During the flexed upstroke the inner, arm wing is drawn close to the body, while the outer, hand wing remains further extended out into the flow. As the wing moves through the horizontal plane in the upstroke at frames c→d, c→d and d→e of Fig. 3A–C, respectively, it is the outer primary wing feathers that are most exposed to the oncoming air. The degree of tail spread decreases with increasing U and the tail is fully furled at the higher flight speeds. It is also notable that the bird has a high body tilt angle at low speeds, but at higher speeds the body is aligned closely with the horizontal; measured tilt angles range between 25° and 10° for flight speeds from 5 to 10 m s^{-1}. The change in wingbeat kinematics and geometry as a function of flight speed U involve incremental changes in the quantitative descriptors of this motion, rather than any sharp qualitative change in the motions themselves.

Time traces describing some of these parameters (vertical position and projected wingspan) can be seen in Fig. 4 for U=10 m s^{-1}. No extra smoothing is imposed on the raw data here, and within the measurement resolution the vertical position is a regular periodic function, which can be quite well fit with a single frequency component sine wave. The projected wingspan is more complex, reflecting the folding of the wing itself. The time traces are quite repeatable over the eight wingbeats shown. The extensive training makes it simple to find useable traces of this kind.

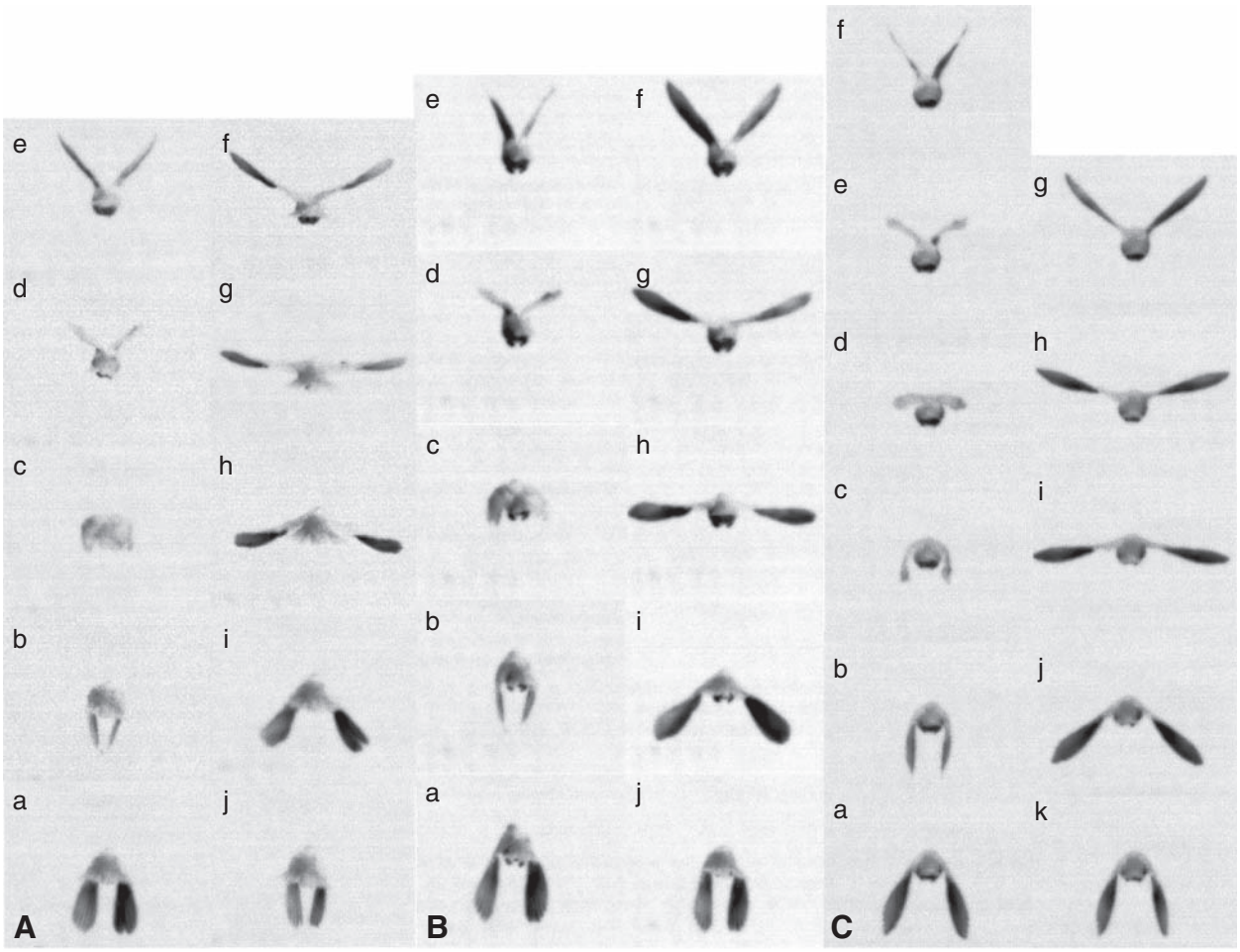

Fig. 3. Rear view of the thrush nightingale in the wind tunnel. Consecutive frames spaced at 0.008 s intervals showing a complete wingbeat at U=5 m s^{-1} (A), 7 m s^{-1} (B) and 10 m s^{-1} (C), starting with the upstroke (a) to the transition between upstroke/downstroke (e,f) and through the downstroke (j) to the transition between downstroke/upstroke.

Wingbeat kinematics from high-speed filming

Timing of the wingbeat cycle

The amplitude of the wingbeat does not change significantly with U (Fig. 5, Table 2). Similarly, the asymmetry of the angular excursion, as measured by A_0, remains almost constant (Table 2). The wingbeat frequency, f, is a very weak U-shape, with a mean of 14.4 Hz and a minimum of 14.0 Hz at 6 m s^{-1} (Fig. 6, Table 2). The overall variation in f is only 7% between the extreme values at 6 and 10 m s^{-1}, respectively.

The successful single frequency sine fit is a consequence of a highly repeatable wing stroke time traces. The 10 point/cycle sampling rate is sufficient to show that smaller scale fluctuations are unlikely to appear in the wingbeat trace. This was tested by approximating the time traces in a Fourier series. The function $z_{tip}(t)$ digitised over N discrete points can be expressed as a discrete sum of Fourier coefficients:

$$Z(i\omega) = \sum_{j=0}^{N-1} z_{tip}(t) e^{i\omega t} \quad . \tag{9}$$

A reconstructed series can then be built from a truncated series of the first nc coefficients only, as:

$$z_r(t) = \frac{1}{2\pi} \sum_{j=0}^{nc} Z(i\omega) e^{-i\omega t} . \tag{10}$$

As nc increases, the difference between z_{tip} and z_r diminishes. If the true kinematics are close to a simple harmonic function, a reasonable approximation can be found from the first term only. The sum of the 0–3 terms from the Fourier series is shown as the solid line in Fig. 7. The time derivative, z_r'' can be calculated by analytical differentiation of the series approximation, and is shown as a broken line. The inflection points at mid up- and downstroke are partly an artefact of the reconstruction from a reduced set of coefficients, but also reflect a departure from pure harmonic motion at the base frequency (Fig. 7).

Since f changes only a little, the reduced frequency k (equation 4) declines systematically with U, ranging from approximately 0.4 to 0.2 over U=5–10 m s^{-1} (Fig. 8).

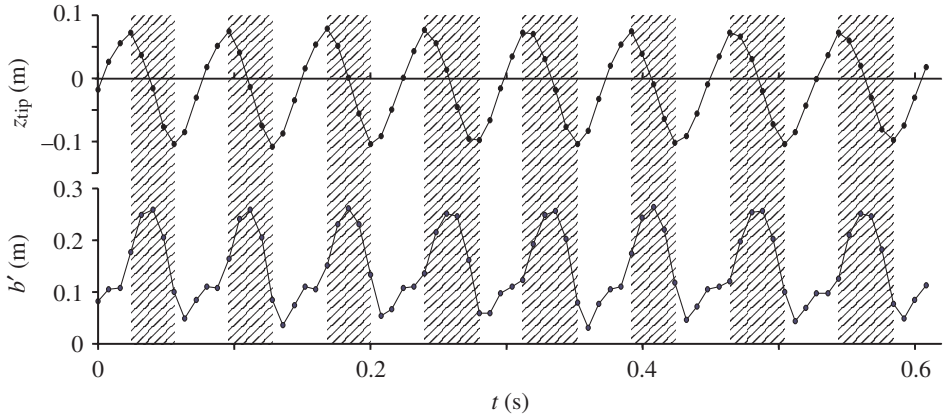

Fig. 4. Eight wingbeats of the thrush nightingale in steady level flight at U=10 m s^{-1}. Here, one typical wingtip tracing is presented as wingtip trace z_{tip} and projected wingspan b'. Downstroke regions are hatched.

Moreover, since A_1, hence ϕ, does not change significantly with U, then $J(U)$ is also a simple function, not significantly different from a straight line, whose constant slope can be predicted from

$$\Delta J / \Delta U = 1 / 2\phi bf\,. \quad (11)$$

Equation 11 evaluates to 0.12 s m^{-1}, and the fitted slope in Fig. 8 is 0.11 s m^{-1}.

In Fig. 9 the vertically and horizontally projected wingtip traces for three different speeds have been plotted side by side to show how the wingbeat patterns vary qualitatively over the speed range. The plots are on a grid with aspect ratio of 1, and show wingtip trace z_{tip} (open circles) and the projected wingspan b' (filled circles) over the course of several wingbeats. Since the wingbeat frequency f is approximately constant (Fig. 6), the wavelength λ of the wingbeat cycle increases with increasing U. In fact, this is the only notable difference between the projected wing traces, which otherwise appear similar in form. The exception to this otherwise geometric similarity is the slightly increased time spent on the upstroke, visible in Fig. 9 as an increasing percentage of non-hatched area, and measured by decreasing downstroke fraction, τ in Fig. 10.

Table 2. *Vertical direction of the wingtip over time as described by a single frequency sine fit*

U (m s^{-1})	N	A_0 (m)	A_1 (m)	f (Hz)
5	5	–0.015	0.075	14.1
6	5	–0.015	0.077	14.0
7	5	–0.016	0.084	14.2
8	4	–0.016	0.079	14.2
9	5	–0.014	0.081	14.8
10	4	–0.014	0.079	15.0
Mean ± S.D.		–0.015±0.001	0.079±0.003	14.4±0.4

Single frequency sine fit, see equation 2.

U, airspeed; N, number of sequences analysed; A_0, offset of wingbeat; A_1, amplitude; f, wing beat frequency.

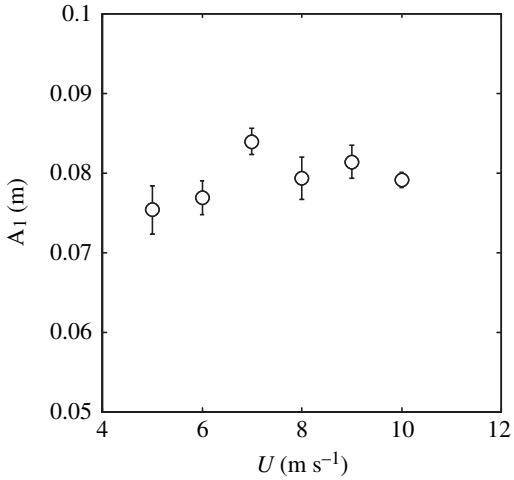

Fig. 5. Amplitude A_1 (m) derived from a single frequency sine fit to the wingtip trace. $2A_1$ represents the peak-to-peak swing of the wingtip over a full wingbeat. There is no significant dependence of A_1 on U. (ANOVA: A_1=0.0009U+0.073; N=28, r^2=0.06, P>0.05). For details see Table 2. Values are means ± S.E.M.

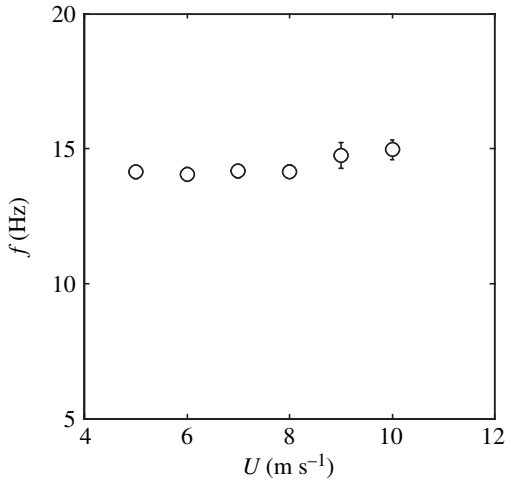

Fig. 6. Wingbeat frequency f (Hz) as function of flight speed U. The variation between maximum and minimum f is small, only 7%. (ANOVA: f=0.060U^2–0.73U+16.25; N=28, r^2=0.18, P<0.05). For details see Table 2. Values are means ± S.E.M.

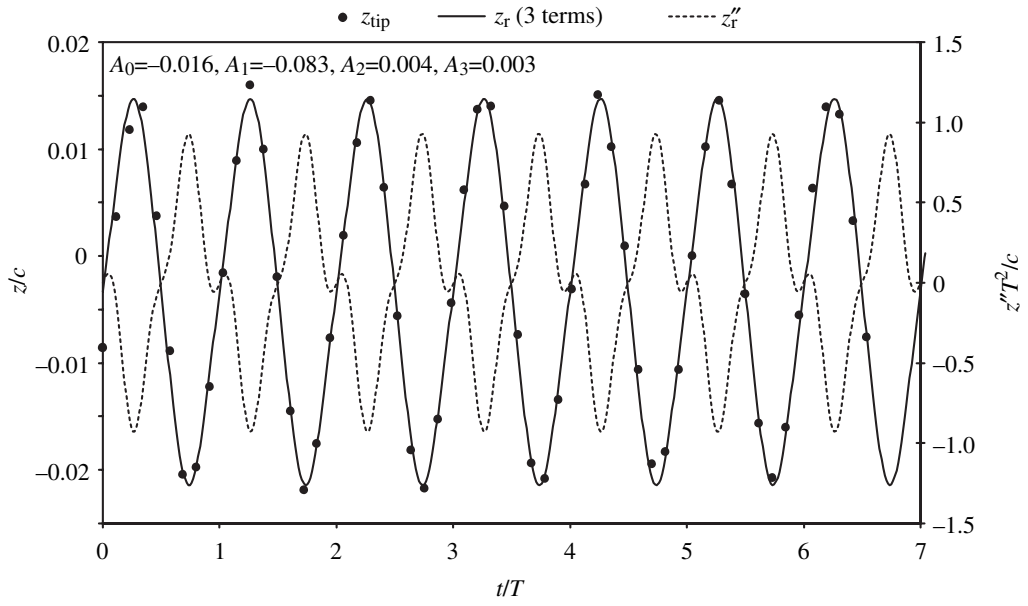

Fig. 7. The solid line shows the Fourier series approximation of the projected wing tip trace (filled circles). The coefficient amplitudes (in m) are given by A_n. The normalised acceleration is shown by the broken line.

The maximum wingspan, measured at mid-downstroke, did not change significantly with flight speed, but the ratio of the span during the upstroke to that of the downstroke increased with increasing speed (Fig. 11).

Kinematics and wakes

Of the primitive kinematics parameters measured in the previous section, the only systematic variations with flight speed were in the downstroke ratio τ, the span ratio *R* and, to some degree, the wingbeat frequency *f*. As far as can be measured from these data, there are no significant quantitative or qualitative changes in wingbeat amplitude and it is only the relative contribution of the upstroke within the wingbeat cycle that can be associated with variation in *U*. This restricted range of variation in kinematics can be linked with measured wake structure.

Fig. 12 shows vertical centre plane cross sections of the wake at flight speeds of 5, 8 and 11 m s^{-1}, complementing those shown in Spedding, Rosén and Hedenström (2003a) given for 4, 7 and 10 m s^{-1}). At *U*=5 m s^{-1}, the downstroke wake is the most notable feature, beginning with a strong cross-stream starting vortex (+ arrow in Fig. 12). By contrast, the stopping vortex (– arrow) is more diffuse and weak. While the upstroke appears to be mostly aerodynamically inactive, as indicated by the low-magnitude induced flow vectors in the upstroke part of Fig. 12, and it was only by including contributions to the total circulation from elements that appear during the upstroke traces that a satisfactory crude balance

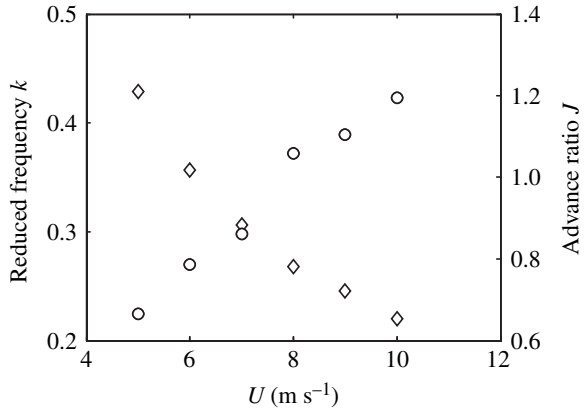

Fig. 8. Reduced frequency *k* (diamonds), and advance ratio *J* (circles), as function of flight speed *U* (m s^{-1}).

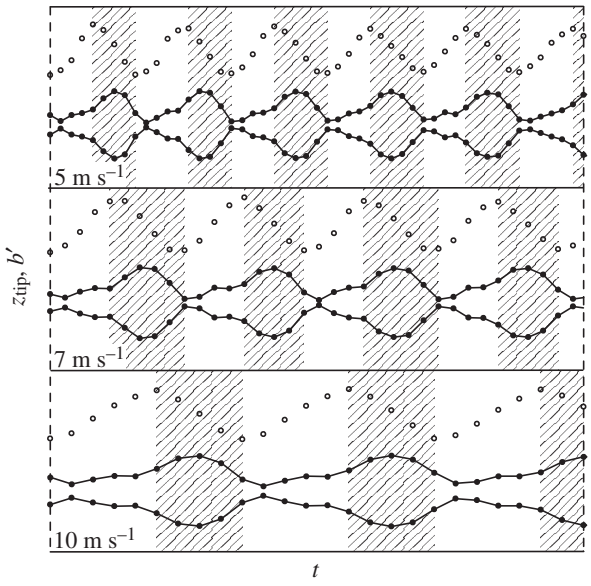

Fig. 9. Wingtip trace z_{tip} (open circles) and projected wingspan b' (filled circles; mean values for both wings are mirrored), over a series of wingbeats at *U*=5, 7 and 10 m s^{-1}. The bird is flying from right to left and all data is to scale on a 2 m×2 m grid. The start and end of a stroke phase is determined by maximum or minimum wingtip position, $z_{tip,max}$ and $z_{tip,min}$. The downstroke phase is hatched. Data sampled at 1/125 s intervals.

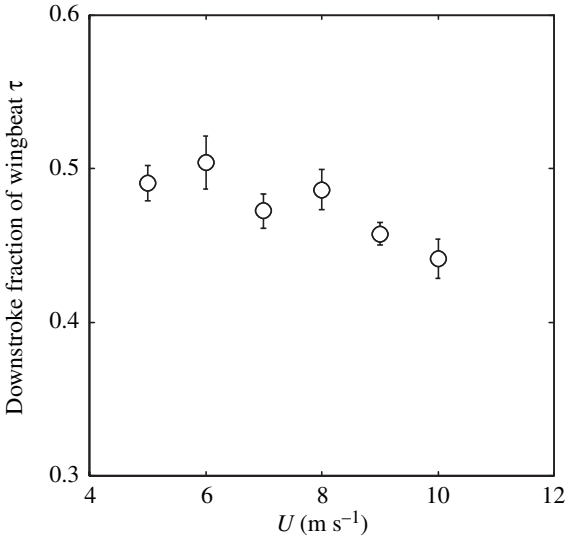

Fig. 10. The downstroke fraction τ of the wingbeat cycle *versus* flight speed, U (m s^{-1}). (ANOVA: τ=–0.011U+0.55; N=28, r^2=0.31, P<0.005). Values are means ± S.E.M.

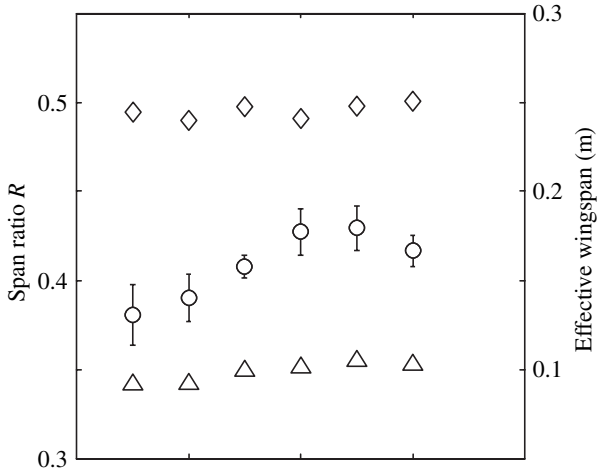

Fig. 11. Span ratio R *versus* flight speed, U (m s^{-1}) (circles, ANOVA: R=–0.009U+0.34; N=28, r^2=0.28, P<0.005) Values are means ± S.E.M. The mid-upstroke wingspan (triangles; ANOVA: N=28, r^2=0.38, P<0.001) and the mid-downstroke wingspan (diamonds; ANOVA: N=28, r^2=0.06, P>0.05) are shown for comparison.

between weight and vertical impulse could be achieved in Spedding, Rosén and Hedenström (2003a). The trace upstroke vorticity in Fig. 12A is thus important.

At 8 m s^{-1} the downstroke again begins with a strong starting vortex, while the stopping vortex and upstroke leave behind a complex pattern of vorticity, which can now be seen throughout the entire upstroke region. The induced flow and its downward component are more noticeable, indicating upstroke generation of lift (at the expense of additional drag).

At 11 m s^{-1} the wake pattern trails through the entire wingbeat, with neither the beginning nor end of the downstroke being particularly distinct. This implies a mode of flight that most closely resembles a constant circulation model, with an aerodynamically loaded wing on both down- and upstroke (Rayner, 1986; Spedding, 1987), although the constant shedding of cross-stream vorticity is not the same as the proposed absence of such shedding in the constant circulation model.

Just as in the kinematics analysis, the most evident qualitative variations in wake structure come from the relative magnitude of the contribution from the upstroke.

Wake geometry

The angle of the induced downwash ψ_{ind}, the actual wake trace ψ_{trace} defined by the core vortex structures, and the path of the wingtip ψ_{kin} as it progresses through the air (equation 8) are presented in Fig. 13A,B (downstroke) and Fig. 13C,D (upstroke). There are significant differences between the kinematics data and the data from the actual wake measurements. Also, the two different wake measurements differ in both upstroke and downstroke. Most of the differences simply show that the wake does not remain frozen in place on the path left by the wing trace. Others indicate interactions between upstroke and downstroke components. These will be discussed in context in the next section.

Discussion

Basic principles

The Joukouski lift, L', per unit span of an aerofoil section is

$$L' = \rho\Gamma U \, . \tag{12}$$

If the lift required is a constant (for steady weight support), then in a constant density (ρ) environment, as U increases the circulation Γ required decreases. The demands on the lifting surface are reduced (the wings can operate at a smaller angle of attack and lift coefficient) because the mass flow available for downward deflection has increased. The same interpretation can be made from the wake. Simplifying greatly, suppose a wing pair of span 2b, moves at speed U, then the area A of a rectangular wake left behind during some characteristic time, T_c, would be A=2bUT_c. The wake impulse over this segment is then

$$I = \rho\Gamma A \, . \tag{13}$$

Because A rises as U increases (the wings are tracing out a larger area per unit time), we arrive at the same conclusion, that Γ need not be so large at high U to provide a given reaction force.

The demands of weight support thus become easier to satisfy as flight speed increases. The drag on the wings and body rises steeply, however (as U^2), and the wings/wake must also generate a net horizontal force to balance the sum of all drag components. In the absence of a separate thrust generator, the wake geometry itself must be arranged to produce the thrust. The differing functions of the downstroke and upstroke account for this.

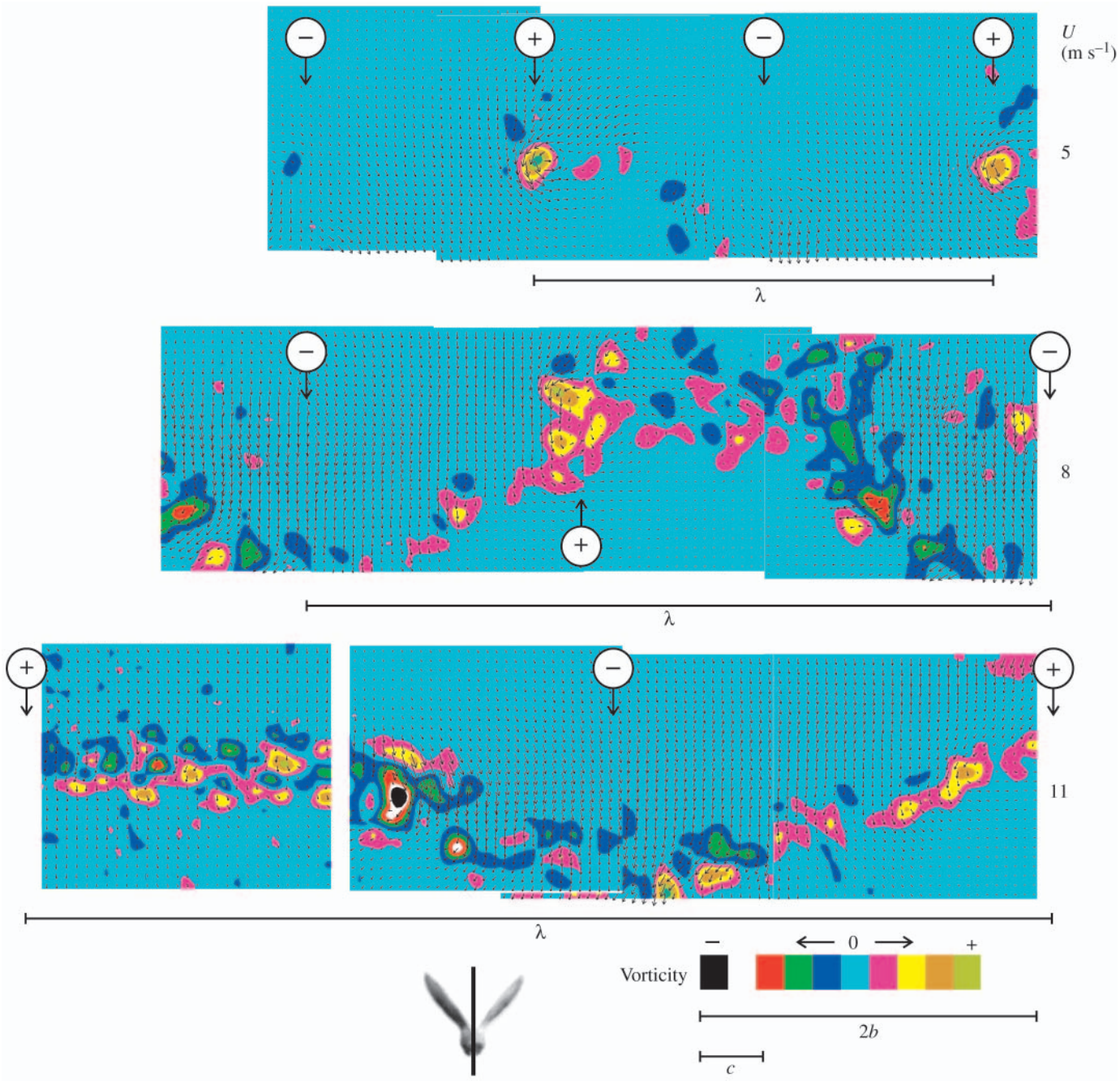

Fig. 12. Composite colour-coded spanwise vorticity with superimposed velocity field vectors for flight speeds U=5, 8 and 11 m s^{-1}. Data are from the vertical centreplane. Velocity vectors are shown at half resolution. The vorticity is mapped symmetrically about a 10-step colour bar. The resolution of the colour bar matches the worst-case uncertainty in the measurement, so all visible features exist. The colour bar is rescaled to local absolute maxima at each different flight speed; these are ±700, 280 and 200 s^{-1}, respectively. The regions corresponding to a starting and stopping vortex are indicated by a (+) and (–) arrow, respectively. The stroke wavelength λ is shown as a black bar and the wingspan, 2b, and mean chord, c, is shown for reference. For more details and examples of wakes at other speeds (4, 7 and 10 m s^{-1}; see Spedding et al., 2003a).

Downstroke ratio decreases with U

The differing roles of the down- and upstrokes were seen in the traces of Fig. 9, and quantitatively in Fig. 10. The downstroke ratio τ decreases significantly from values of close to 0.5 at low speed to about 0.45 at high speeds. At low speeds, the largest contributor to weight support is the downstroke, which is responsible for the generation of a large-scale structure with properties similar to a vortex loop (Spedding, Rosén and Hedenström, 2003a). This structure lies at a relatively small angle to the horizontal (Fig. 13B), and so most

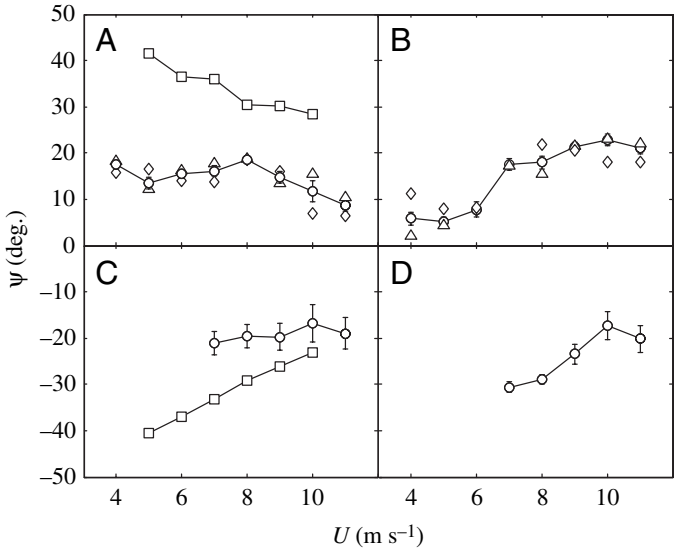

Fig. 13. (A) Inclination angles for downstroke: ψ_{kin} (squares; N=28, see equation 8) and ψ_{ind} from body centre position (diamonds, N=63) and mid-wing position (triangles; N=95) with a mean value of (circles; N=158). (B) ψ_{trace} from downstroke measured at body centre position (diamonds, N=28) and mid-wing position (Δ, N=86) and mean values (circles; N=122). (C) Upstroke inclination angles for: ψ_{kin} (squares; N=28) and ψ_{ind} from body centre position (circles; N=47). (D) ψ_{trace} for downstroke measured at body centre position (circles; N=52). Values are means, and means ± S.E.M.

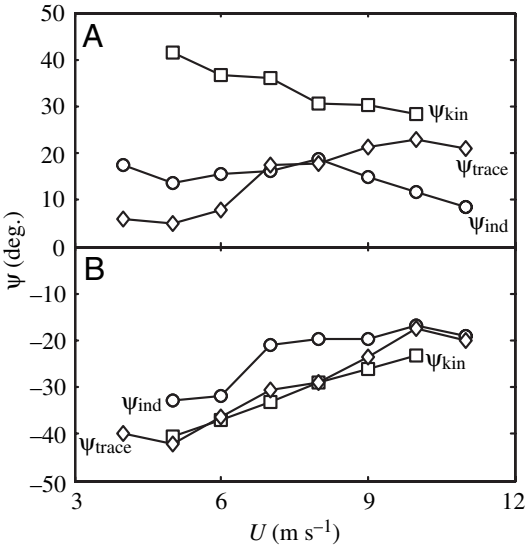

Fig. 14. Summary of wake geometry data (abstracted from Fig. 13). (A) Downstroke, (B) upstroke. Squares, ψ_{kin}; circles, ψ_{ind}; diamonds, ψ_{trace}.

of the impulse, directed normal to the plane of the structure, points upwards. The forward component is comparatively small because at low speeds the total viscous and pressure drags are also small. The direct contribution of the upstroke to weight support is difficult to ascertain (Spedding, Rosén and Hedenström, 2003a), but it appears not to be zero. Nevertheless, a large drag penalty from an exotic upstroke motion cannot be balanced by the downstroke structure, and so the direct contribution of the upstroke to weight support can be inferred to be small. As U increases, the downstroke can more readily provide an increasing thrust component, while the upstroke assumes a more significant role in weight support. As the wake structures left behind during the upstroke become more evident (Spedding, Rosén and Hedenström, 2003a; Fig. 12), it occupies a larger fraction of the total wingbeat.

A decrease of τ with increasing U has been observed also in other species (Park et al., 2001; Tobalske and Dial, 1996), and even if the absolute range of τ varies between species it commonly starts at about 0.5 at the slowest flight speeds measured in a wind tunnel.

Geometry of the wake and its induced flow

Following the classical textbook treatments, where a velocity field can be conveniently described as the flow induced by the presence of a certain distribution of vortex elements, one searches for similar experimental descriptions of the measured flows. In Spedding, Rosén and Hedenström (2003a), it was noted that the true wake flows behind a flapping bird were complex and the most appropriate reduction of the velocity fields to simpler forms generated by a small number of vortex lines in three dimensions was an intricate exercise.

To make a correspondence between wing kinematics and wake structure, a simpler data subset is considered here; only the vertical centreplane velocity fields and their associated spanwise vorticity distributions, as in Fig. 12. Fig. 14 summarizes the three different wake inclination angles, ψ_{ind}, ψ_{trace} and ψ_{kin}, for the downstroke and upstroke, as a function of flight speed U, condensing the full measurements of Fig. 13.

In the downstroke (Fig. 14A), all three angles have measurably different trends with increasing U, but the same measures from the upstroke (Fig. 14B) are similar in both sign and magnitude. The differences in downstroke can be explained in a qualitative manner in two steps.

(1) $\psi_{trace} \neq \psi_{kin}$. Since the relative changes in both wingbeat frequency f (Fig. 6) and downstroke ratio τ (Fig. 10) are small compared with $\Delta U/\overline{U}=2/3$ [where $\overline{U}$ is a characteristic flight speed, e.g. $(U_{max}-U_{min})$, the advance ratio, $J=1/K$, increases almost in direct proportion to U, and the inclination angle of the path of the wingtip trace, ψ_{kin}, decreases similarly. The decrease of ψ_{kin} with U is a poor predictor, however, of the position of the vortex wake structure as measured by ψ_{trace}, which increases with U. First, we note that the wake structure is measured about 17.5 chord lengths downstream from the bird and so represents the pattern as the flow has evolved over about 2.4λ at 5 m s^{-1} and 1.3λ at 10 m s^{-1} (or 2.4T and 1.3T, respectively). During this time, the wake has moved by self-induced convection, downwards from its starting point; let us denote the vertical component of this velocity w_{self}. Since the starting vortex is created first in the wingbeat cycle, at any later time it has had longer to move than other parts, and ψ_{trace}, measured under the connecting line from start vortex to stop

vortex, will always be lower than the trace of the wingtip ψ_{kin}. At the lowest flight speed of 5 m s^{-1}, the strength of shed vortices is higher, induced downwash velocities are higher, and w_{self} will be higher compared with the forward speed. As U increases, wake element circulations decrease, and the ratio w_{self}/U decreases rapidly. At U_{max}, ψ_{trace} is almost equal to ψ_{kin}, approaching it from below.

(2) ψ_{ind} is derived from the mean measured downwash angle at the mid-point of a wake element. At low flight speeds, the downwash is tilted further aft than would be inferred from the isolated wake vorticity (at the centreplane only) left behind during the downstroke. The arguments for the measured ψ_{trace}, based mainly on self-induced wake motion, do not apply because the trend for ψ_{ind} is opposite; it starts higher than ψ_{trace} and then declines with increasing U.

There is no simple correlate with the measured wingbeat kinematics to explain the magnitude and trend of $\psi_{ind}(U)$. Spedding, Rosén and Hedenström (2003a) reported no significant out-of-plane deformations of the inferred 3D wake structures, even though the supporting data are sparse. There are no obvious trends with amplitude (Fig. 5) or stroke plane inclination angle (M.R., G.R.S. and A.H., unpublished data from high-speed side-view sequences) to indicate a commensurate change in large-scale kinematics, which would then in any case be inconsistent with the previous discussion of ψ_{trace} *vs.* ψ_{kin}.

Fig. 3 shows a strong pronation of the leading edge during mid-downstroke for all three flight speeds (Fig. 3Ai, Bh, Ci). The middle case (7 m s^{-1}) has the largest projected area of the wing on to the image plane. Strong pronation will lead to an effective aerodynamic angle of attack that gives a backward component to the induced downwash. As U increases, this component will become comparatively smaller, and so the net downwash angle should increase, decreasing ψ_{ind}. The decrease of ψ_{ind} is actually delayed until middle-range flight speeds, due to the increased pronation up to that point. Lacking detailed data on the 3D flow field close to the wing and on similar details of the wing kinematics, these explanations are speculative. Nevertheless, the trend of $\psi_{ind}(U)$ seems very likely to be linked most closely with variations in the effective local angle of attack of the wing, and it would be interesting to know more.

The upstroke wake angles in Fig. 14B all decrease in magnitude with decreasing U. The same considerations apply as for the corresponding downstroke angles (with appropriate changes in sign), but since the wake flow is weaker, then so are departures due to self-deformation or convection. ψ_{ind} is consistently smaller in magnitude at lower flight speeds (closer to horizontal) than both ψ_{trace} and ψ_{kin}, and the explanation is again likely to be related to details of effective angle of attack during the upstroke.

While the relationships between ψ_{trace}, ψ_{ind} and ψ_{kin} are not completely obvious *a priori*, they can be understood in a consistent way. They are clearly significantly different from the most simple ideas about wingbeat kinematics and aerodynamics – the vortex wake does not lie frozen along the wingtip trace, the downwash is not normal to the plane of the wake and the wake structure could not readily be predicted or inferred from the wing motions alone. Appropriate and as-yet-unrealizable computations would be required to properly calculate the unsteady flow field. When that time arrives, data such as these can serve as diagnostics for comparison.

Span ratio and wing flexing

One measure that characterises the unusually flexible geometry of bird wings is the span ratio R. It increases linearly with U (Fig. 11), and its effect can be seen qualitatively in Fig. 9. Flexion of the wing during the upstroke is thought to be essential in providing positive thrust in cruising flight and in avoiding excess drag in slow speed flight. The wake measurements in Spedding, Rosén and Hedenström (2003a) and Fig. 12 suggest a lifting upstroke at most flight speeds and this is supported by the gradual increase of R with U in Fig. 11. This idea is consistent with the corresponding decrease of τ with U in Fig. 10. The mid-downstroke effective wingspan does not change significantly with U but the mid-upstroke does, so the change in R is mostly related to changes in the upstroke (see Fig. 11).

R is also reported to increase with U in the black-billed magpie *Pica pica*, pigeon *Columba livia*, ringed turtle-dove *Streptopelia risoria* and cockatiel *Nymphicus hollandicus* (Tobalske and Dial, 1996; Hedrick et al, 2002). This simple relationship is not universal, however. In the case of the barn swallow *Hirundo rustica*, R has been observed to decrease with U. R falls from 0.5 to 0.15 at flight speeds between 4 and 13 m s^{-1} (Park et al., 2001). Both the morphology and flight of the barn swallow are very different from that of the thrush nightingale (the swallow is lighter, with thinner, more pointed wings; wing loading Q=13 N m^{-2}; AR=7.4). The barn swallow is adapted for slow manoeuvring flight and exhibits an intermittent flight style with a characteristic wingbeat pause at high speed, which is not present in the thrush nightingale. The morphological and behavioural differences ought to be manifest in the wake structure and it would be useful to conduct combined wake and kinematic studies such as the present study on the barn swallow, partly to provide a test of the generality of the conclusions for the thrush nightingale wake.

Not only does the projected wingspan change between downstroke and upstroke, the relative folding of the wing also changes. The most notable difference is that the primary wing feathers are more exposed to the oncoming air than the arm section of the wing in the flexed upstroke. It is usually assumed that the inner part of the wing is responsible for most of the active aerodynamics generated in the upstroke. Here it appears that when any part of the wing is aerodynamically active during the upstroke in the thrush nightingale, it is the hand section of the wing (e.g. Fig. 3). The notion of the importance of the arm wing for the upstroke circulation originates from an analysis of the wake of a kestrel in flapping flight where the arm evidently was important (Spedding, 1987), and this idea agreed well with long-standing kinematic data (Brown, 1953). The results presented here suggest a more varied phenomenon.

Frequency is near constant

The wingbeat frequency is relatively constant, with only a weak U-shape across the speed range (Fig. 6). This feature of thrush nightingale flight was also reported by Pennycuick et al. (1996). Consequently, reduced frequency parameters such as k and J (equations 4, 7) cannot be constant. That is indeed shown in Fig. 8, where k decreases and J increases, both almost linearly with increasing U. Apparently it is unimportant for the bird to maintain a constant reduced frequency over its range of flight speeds, and there is no attempt to adjust f and/or A_1 to achieve even short ranges of constant k or J. The ratio of timescales between stroke period and a mean flow convective time does not seem to be the determining factor in selection of flapping frequency.

A number of theoretical models predict optimal reduced frequencies for flapping flight. In a 2D, direct numerical simulation about pitching and rotating wing segments at Reynolds number $Re=10^3$, Wang (2000) finds an optimal reduced frequency equivalent to $k\approx0.2$ for values of $K=1/J\geqslant0.2$, or $J<5.0$. k and J are never this low for thrush nightingale flight (Fig. 8). Hall et al. (1997) constructed an unsteady inviscid model (with quasi steady viscous corrections) for large amplitude flapping flight and showed optimal advance ratios of between $\frac{1}{2}$ and $\frac{1}{4}$ for minimum power loss. This translates to $0.3<J<0.4$ for our definition of J, which is based on ϕ rather than fixed 2π as an amplitude measure. The optimal values of k and J produced by these different formulations are quite close to each other, although, as noted by Wang (2000), it is not clear why this should be. In Wang's simulation the optimal frequency is determined by natural timescales of growth and shedding of both leading and trailing edge vortices. The result of Hall et al. (1997) also concerns a ratio of advective to wing cycle times, but for entirely different reasons as there are no separation vortices in their inviscid model. In the thrush nightingale the measured value of k never falls to Wang's optimum of 0.2 and J does not fall to the 0.3–0.4 range predicted by Hall et al. (1997).

The perils in simply comparing apparently similar values of a reduced frequency parameter are further illustrated by reference to the thorough and careful analysis of Lewin and Haj-Hariri (2003). In a numerical solution of the 2D flow around a heaving aerofoil they define a usual Strouhal number St by

$$St = fA_{\mathrm{w}} / U \,, \tag{14}$$

where all the symbols have their usual meanings and A_{w} is the wake amplitude, from vortex peak to vortex peak. It is related here to the half-wingbeat amplitude very approximately as $A_{\mathrm{w}}=2A_1$. The authors carefully describe the dependence of their solutions on k and St, and find a broad optimum range of St between 0.3 and 0.5. Defined similarly, $St=0.46$ at $U=5$ m s^{-1} and $St=0.23$ at $U=10$ m s^{-1} here. The numbers are seemingly in agreement. However, St is essentially proportional to the product of k and a heaving (or flapping amplitude). In Lewin and Haj-Hariri (2003), k ranges from 2 to 10, and here k ranges from 0.42 to 0.84. The flapping frequencies are much lower, but amplitudes are much higher, and similar values of St do not necessarily entail similar values of k. Lewin and Haj-Hariri point out that neither St nor k, by themselves, are sufficient to characterise the different flow regimes (also noted and investigated by Jones et al., 1996; Jones and Platzer, 1997), and so once again, some caution is required in interpretation.

It would be extremely interesting if the thrush nightingale were found to be operating at a preferred reduced frequency, because it would imply a close coupling or resonance between fluid dynamical timescales of the mean and fluctuating motions. Then the notion of preferred wingbeat kinematic styles might be supportable. However, the constant frequency data do not show this. The fact that the wingbeat frequency of the thrush nightingale only varies by 7% over the range of U investigated suggests that other factors ultimately dictate the frequency selection. These might include preferred strain rates in muscles and tendons, preferred mechanical resonances dictated by the morphology, or preferred parameter ranges in the associated physiological systems.

The wingbeat frequency of a thrush nightingale studied at the same facility in Lund by Pennycuick et al. (1996) showed a similarly weak dependence on U. The slightly lower absolute values of f are consistent with the 10% smaller mass.

Concluding remarks

This paper serves both as a record of the wing kinematics that produce the wake structures observed in Spedding, Rosén and Hedenström (2003a) and also as corroborating evidence for some of the points discovered there. [Note that it is not an exhaustive attempt to quantify all aspects of thrush nightingale kinematics but is restricted to a dataset that can be compared to the wake data presented in Spedding, Rosén and Hedenström (2003a).] One notable feature of both the wake studies and the associated wing kinematic parameters is the absence of any sign of a discontinuous or sudden variation in any of the measured quantities with U. Much speculation has arisen concerning the possible existence of gaits in animal flight (Rayner, 1993; Tobalske, 2000; Hedrick et al., 2002), but none of the quantitative experimental data covering a continuous range of flight speeds (as opposed to one or two instances) show any measured quantity with abrupt variation, commensurate with some qualitative change in flight style. The data from this paper, and its companion wakes study (Spedding, Rosén and Hedenström, 2003a) are the only source of quantitative data for aerodynamic measurements at more than one single flight speed, and offer no support for the notion of gaits. If it seems convenient to continue to describe categories such as 'slow flight' and 'fast flight', it should be noted that there is no particular (aerodynamic, mechanical, physiological) reason for singling out two, or any other number, of discrete conditions that appear simply as points on a smoothly varying continuum. If behavioural and/or ecologically interesting points are identified, such as minimum power speed, or maximum range speed, then these occur because of their location on equally smooth curves that predict or measure mechanical or metabolic power requirements, and

not because they represent qualitatively different wake structures or wing kinematics.

The variations observed in overall wake geometry can be explained by, or at least reconciled with, the overall wing kinematic data, although observed wake structures and their position would not be easy to deduce from the kinematics alone.

Technology does not yet permit time-resolved, 3D DPIV studies of the wake at these flow speeds, and safety considerations limit the proximity of the bird (and its field of vision) to the laser light sheet. As a result, some care and caution is required in making limited inferences back from some complex flow structure to conditions on the wing when it was originally created.

One feature of the wake that is not yet adequately explained through the available kinematic data is the strong asymmetry between starting and stopping vortices at the beginning and end of the downstroke. This asymmetry has been noted in all quantitative wake studies of slow speed flapping flight (Spedding et al., 1984, 2003a,b; Spedding, 1986) but cannot be readily identified with a similar asymmetry in the wingbeat. Fig. 3 shows that the wings meet much closer together at the end of the downstroke than after the upstroke and interference between the wings and the shed vorticity was suggested by Spedding (1986). Fig. 7 shows that acceleration magnitudes of the wingtip do not differ at the end of each half-stroke. The diffuse distribution of vorticity produced at the end of the downstroke, at the very least, is a significant nuisance in calculating wake-based force estimates (Spedding et al., 2003a) and the story of its origin is likely to be interesting.

Finally, as in Spedding et al. (2003a), we should recall that these conclusions have been obtained from studies in just one species, and the generality of the results is not yet clear. The success of the present work in associating many wake features with their generating kinematic conditions bodes well for future studies using other wing geometries and kinematics.

This work was supported by the Knut and Alice Wallenberg foundation, Carl Tryggers foundation and the Swedish Research Council (to A.H.). The experiments were carried out under licence from the Lund/Malmö Ethical Committee.

List of symbols

A	area
A_1	amplitude
A_o	offset of amplitude
A_w	wake amplitude
$\mathcal{AR}$	aspect ratio
b	semi wingspan
b'	projected wingspan
c	mean chord
f	wingbeat frequency
$\boldsymbol{g}$	acceleration due to gravity
I	wake impulse
J	advance ratio
K	reduced frequency based on wingtip speed
k	reduced frequency based on mean wing chord
L'	lift per unit span
m	body mass
Q	wing loading
R	span ratio
Re	Reynolds number
S	wing area
s	arc length
St	Strouhal number
T	stroke period
T_c	characteristic time
t	time
U	flight speed
w_{self}	vertical component of self-induced convection
w_{tip}	vertical wingtip velocity
z_{tip}	vertical wingtip position
Z_r	approximation of z_{tip}
Γ	circulation
ϕ	stroke angle
φ	phase offset
λ	stroke wavelength
ρ	air density
τ	downstroke fraction of wingbeat
ω	radian frequency
ψ_{ind}	inclination angle of induced flow
ψ_{kin}	inclination angle of wingtip trace
ψ_{trace}	inclination angle of wake trace

Subscripts u and d denote upstroke and downstroke, respectively.

References

Brown, R. H. J. (1953). The flight of birds. II. Wing function in relation to flight speed. *J. Exp. Biol.* **30**, 90-103.

Hall, K. C., Pigott, S. A. and Hall, S. R. (1997). Power requirements for large-amplitude flapping flight. *AIAA* 97-0827.

Hedrick, T. L., Tobalske, B. W. and Biewener, A. A. (2002). Estimates of circulation and gait change based on a three-dimensional kinematic analysis of flight in cockatiels (*Nymphicus hollandicus*) and a ringed turtle-doves (*Streptopelia risoria*). *J. Exp. Biol.* **205**, 1389-1409.

Jones, K. D. and Platzer, M. P. (1997). Numerical computation of flapping wing propulsion and power extraction. *AIAA* 97-0826.

Jones, K. D., Dohring, C. M. and Platzer, M. P. (1996). Wake structures behind plunging airfoils: a comparison of numerical and experimental results. *AIAA* 96-00078.

Lewin, G. C. and Haj-Hariri, H. (2003). Modelling thrust generation of a two-dimensional heaving airfoil in a viscous flow. *J. Fluid Mech.* **492**, 339-362.

Moreau, R. E. (1972). *The Palearctic-African Bird Migration Systems.* London: Academic Press.

Norberg, U. M. (1976). Kinematics, aerodynamics and energetics of horizontal flapping flight in the long-eared bat (*Plecotus auritus*). *J. Exp. Biol.* **65**, 179-212.

Park, K. J., Rosén, M. and Hedenström, A. (2001). Flight kinematics of the barn swallow *Hirundo rustica* over a wide range of speeds in a wind tunnel. *J. Exp. Biol.* **204**, 2741-2750.

Pennycuick, C. J., Klaassen, M., Kvist, A. and Lindström, Å. (1996). Wingbeat frequency and the body drag anomaly: wind tunnel observations on a thrush nightingale (*Luscinia luscinia*) and a teal (*Anas crecca*). *J. Exp. Biol.* **199**, 2757-2765.

Pennycuick, C. J., Alerstam, T. and Hedenström, A. (1997). A new low-

turbulence wind tunnel for bird flight experiments at Lund University, Sweden. *J. Exp. Biol.* **200**, 1441-1449.

Rayner, J. M. V. (1986). Vertebrate flapping flight mechanics and aerodynamics, and the evolution of flight in bats. In *Biona Report*, vol. 5 (ed. W. Nachtigall), pp. 27-74. Stuttgart: Gustav Fischer Verlag.

Rayner, J. M. V. (1993). On aerodynamics and the energetics of vertebrate flapping flight. *Cont. Math.* **141**, 351-400.

Spedding, G. R. (1986). The wake of a jackdaw (*Corvus monedula*) in slow flight. *J. Exp. Biol.* **125**, 287-307.

Spedding, G. R. (1987). The wake of a kestrel (*Falco tinnunculus*) in flapping flight. *J. Exp. Biol.* **127**, 59-78.

Spedding, G. R. (1993). On the significance of unsteady effects in the aerodynamic performance of flying animals. *Cont. Math.* **141**, 401-419.

Spedding, G. R., Rayner, J. M. V. and Pennycuick, C. J. (1984). Momentum and energy in the wake of a pigeon (*Columba livia*) in slow flight. *J. Exp. Biol.* **111**, 81-102.

Spedding, G. R., Rosén, M. and Hedenström, A. (2003a). A family of vortex wakes generated by a thrush nightingale in free flight in a wind tunnel over its entire natural range of flight speeds. *J. Exp. Biol.* **206**, 2313-2344

Spedding, G. R., Hedenström, A. and Rosén, M. (2003b). Quantitative studies of the wakes of freely-flying birds in a low turbulence wind tunnel. *Exp. Fluids* **34**, 291-303.

Theodorsen, T. (1934). General Theory of Aerodynamic Instability and the Mechanism of Flutter. *NACA* TR 496.

Tobalske, B. W. (2000). Biomechanics and physiology of gait selection in flying birds. *Physiol. Biochem. Zool.* **73**, 736-750.

Tobalske, B. W. and Dial, K. P. (1996). Flight kinematics of black-billed magpies and pigeons over a wide range of speeds. *J. Exp. Biol.* **199**, 263-280.

Wang, J. Z. (2000). Vortex shedding and frequency selection in flapping flight. *J. Fluid Mech.* **410**, 323-341.